Sub-annual and seasonal variability of Atlantic-origin waters in two adjacent west Greenland fjords

D. Carroll[1], D. A. Sutherland[2], B. Curry[3], J. D. Nash[4], E. L. Shroyer[4], G. A. Catania[5,6], L. A. Stearns[7], J. P. Grist[8], C. M. Lee[3], and L. de Steur[9,10].

[1]Jet Propulsion Laboratory, California Institute of Technology, Pasadena, California, USA.
[2]Department of Earth Sciences, University of Oregon, Eugene, Oregon, USA.
[3]Applied Physics Lab, University of Washington, Seattle, Washington, USA.
[4]College of Earth, Ocean and Atmospheric Sciences, Oregon State University, Corvallis, Oregon, USA.
[5]Department of Geological Sciences, University of Texas at Austin, Austin, Texas, USA.
[6]Institute for Geophysics, University of Texas at Austin, Austin, Texas, USA.
[7]Department of Geology, University of Kansas, Kansas, USA.
[8]National Oceanography Centre, University of Southampton Waterfront Campus, European Way Southampton, SO14 3ZH, UK
[9]Norwegian Polar Institute, Tromsø, Norway.
[10]Royal Netherlands Institute for Sea Research (NIOZ), Den Burg, Netherlands.

Corresponding author: Dustin Carroll (dustin.carroll@jpl.nasa.gov)

Key Points:

- We analyze a two-year hydrographic record from a suite of moorings in Davis Strait and two adjacent west Greenland fjords
- Hydrography above the sill exhibits clear seasonality; sub-annual warming of basin waters coincides with the arrival of dense Atlantic-origin waters at the mouth
- We use Seaglider observations and reanalysis of sea-ice and winds to explore the role of local and remote forcing in driving fjord renewal

Abstract

Greenland fjords provide a pathway for the inflow of warm shelf waters to glacier termini and outflow of glacially-modified waters to the coastal ocean. Characterizing the dominant modes of variability in fjord circulation, and how they vary over sub-annual and seasonal timescales, is critical for predicting ocean heat transport to the ice. Here we present a two-year hydrographic record from a suite of moorings in Davis Strait and two neighboring west Greenland fjords that exhibit contrasting fjord and glacier geometry (Kangerdlugssuaq Sermerssua and Rink Isbræ). Hydrographic variability above the sill exhibits clear seasonality, with a progressive cooling of near-surface waters and shoaling of deep isotherms above the sill during winter to spring. Renewal of below-sill waters coincides with the arrival of dense waters at the fjord mouth; warm, salty Atlantic-origin water cascades into fjord basins from winter to mid-summer. We then use Seaglider observations at Davis Strait, along with reanalysis of sea-ice and wind stress in Baffin Bay, to explore the role of the West Greenland Current and local air-sea forcing in driving fjord renewal. These results demonstrate the importance of both remote and local processes in driving renewal of near-terminus waters, highlighting the need for sustained observations and improved ocean models that resolve the complete slope-trough-fjord-ice system.

1 Introduction

Ocean heat transport to marine-terminating glaciers has been identified as a potential mechanism for dynamic mass loss of the Greenland Ice Sheet [Joughin et al., 2012; Straneo and Heimbach, 2013], with interannual variability in the large-scale ocean circulation and Greenland boundary current system thought to have triggered increased submarine melting of glacier termini [Holland et al., 2008]. Along the ice sheet periphery, sub-annual fjord-scale processes [Straneo and Cenedese, 2014] provide a mechanism for propagating longer-term changes in offshore waters to the ice. Therefore, sustained ocean observations that resolve sub-annual and seasonal variability in fjord hydrography and circulation [Jackson et al., 2014, 2016; Mortensen et al., 2014] are necessary for understanding both the fjord and glacier response to variations in large-scale ocean forcing.

Several key fjord-scale processes have been previously identified [Mortensen et al., 2011; Jackson et al., 2014] as mechanisms for the transport of warm shelf waters to glacier termini over sub-annual and seasonal timescales: 1) estuarine and subglacial discharge-driven circulation, 2) intermediary circulation, 3) along-fjord wind forcing, and 4) dense coastal inflows. Estuarine and subglacial discharge-driven circulation results from the injection and mixing of liquid freshwater into fjords by terrestrial runoff, subglacial discharge [Xu et al., 2012; Sciascia et al., 2013; Carroll et al., 2015, 2016], and submarine iceberg [Enderlin et al., 2016; Moon et al., 2017] and terminus melt [Slater et al., 2015]. Previous observational and modeling work indicates that subglacial discharge circulation can draw shelf waters over sills and renew fjord basins over seasonal timescales [Gladish et al., 2015a; Carroll et al., 2017]. Intermediary circulation results from above-sill isopycnal displacement at the fjord's mouth, which can occur at any frequency, or aperiodically [Aure and Stigebrandt, 1990; Aure et al., 1996]. In southeast Greenland, strong barrier winds [Jackson et al., 2014, 2016] and variability in the East Greenland Coastal Current [Harden et al., 2014] can drive fluctuations in the coastal pycnocline, allowing for rapid fjord-shelf exchange when subglacial discharge circulation is inactive or weak [Straneo et al., 2010; Jackson et al., 2016]. For fjords with intense tidal mixing, heat and freshwater can be mixed downward in the water column, resulting in intermediary circulation within the fjord [Mortensen et al., 2011]. Along-fjord wind forcing has been shown to enhance estuarine [Svendsen and Thompson, 1978; Moffat, 2014] and subglacial circulation [Carroll et al., 2017], with katabatic wind events allowing for roughly 10% of surface waters to be flushed out of the fjord [Spall et al., 2017]. Dense coastal inflows are episodic gravity currents that can cascade over sills and renew basin waters [Edwards and Edelsten., 1977; Mortensen et al., 2014; Gladish et al., 2015a,b], typically lasting several months per event [Mortensen et al., 2011]. Ultimately, assessing the influence of these disparate processes, which have distinct magnitudes and timing across the parameter space of Greenland fjords, is necessary in order to understand how offshore signals are transported to glacier termini.

While these previous efforts have been useful in identifying discrete modes of fjord circulation, we still lack an understanding of how variability in the Greenland boundary current system [Myers et al., 2007; Harden et al., 2014; Grist et al., 2014; Rykova et al., 2015] influences these small-scale fjord processes, and thus, sub-annual and seasonal variability in submarine melt rates and glacier behavior [Moon et al., 2014, 2015]. The complex network of submarine troughs, canyons, and sills that connect the 200+ Greenland outlet glaciers to the shelf [Rignot et al., 2016a; Fenty et al., 2017; Morlighem et al., 2017] suggest that shelf waters may be significantly modulated by localized bathymetry and cross-shelf exchange processes. Additionally, neighboring Greenland fjords often contain glaciers grounded at different depths, exposing termini to contrasting ocean temperatures despite similar water properties at the fjord mouths [Porter et al., 2014; Bartholomaus et al., 2016]. Finally, ocean data from Greenland fjords are heavily biased towards summer observations. Therefore, time-series data are critical for providing context for how these summer observations, which are often synoptic, fit into the framework of sub-annual and seasonal fjord dynamics. Without detailed knowledge of how water properties are modified across the complete shelf-trough-fjord-ice system, our ability to couple ice sheet models to large-scale ocean models, which typically do not resolve trough and fjord-scale processes, remains problematic. These deficiencies highlight the need for coupled shelf and fjord observations, which are critical for quantifying the net annual ocean heat transport to the ice, estimating iceberg and terminus melt rates, and connecting sub-annual and seasonal fluctuations in glacier behavior to shelf water properties.

Here we use a two-year hydrographic record from a suite of moorings in Davis Strait and two adjacent west Greenland fjords (Kangerdlugssuaq Sermerssua and Rink Isbræ, henceforth referred to as “KS” and “Rink”) to investigate sub-annual and seasonal variability in shelf and fjord water properties. We show that hydrographic variability above the sill depth in these fjords exhibits a clear seasonal cycle, with the sub-annual renewal of below-sill waters coinciding with the arrival of dense Atlantic-origin waters at the fjord mouth. We then use Seaglider and shipboard observations from Davis Strait, along with reanalysis of sea-ice cover and wind stress in Baffin Bay, to explore the role of the West Greenland Current and local air-sea forcing in driving fjord renewal.

2 Study area and methods

2.1 Physical setting

Baffin Bay is a semi-enclosed, seasonally ice-covered basin that separates west Greenland and Baffin Island (Figure 1a). It is connected to the Atlantic Ocean by a ~640-m deep sill at Davis Strait [Curry et al., 2011, 2014] and the Arctic Ocean through the complex network of basins and straits that form the Canadian Arctic Archipelago (CAA) [Melling, 2000]. Baffin Bay has a maximum depth of ~2370 m [Tang et al., 2004], with a relatively wide, gently-sloping shelf to the west of Greenland and a narrow, steep shelf off Baffin Island. Mean circulation in Baffin Bay is cyclonic [Dunlap and Tang, 2006], consisting of the cold and fresh southward-flowing Baffin Island Current (BIC) and the northward flowing West Greenland Current (WGC) [Cuny et al., 2002] (Figure 1a).

Following Curry et al. [2014], we define four primary water masses in Baffin Bay: 1) Arctic Water (AW; $\theta \leq 2$°C; $S \leq 33.7$), 2) West Greenland Shelf Water (WGSW; $\theta < 7$°C; $S < 34.1$), 3) West Greenland Irminger Water (WGIW; $\theta > 2$°C; $S > 34.1$), and 4) Transitional Water (TrW; $\theta > 2$°C; $S > 33.7$). Low-salinity AW flows southward in the BIC at depths between ~100–300 m and results from mixing between the upper layer of water entering Baffin Bay on the eastern side of Davis Strait and inflow from the CAA. AW is cooled during winter as it circulates around Baffin Bay and is modified by sea-ice formation and melt, solid and liquid discharge from Greenland and CAA glaciers, and local air-sea fluxes. WGSW consists of Arctic-origin water that is influenced by glacial runoff and sea-ice processes as it flows northward in the upper ~100 m along the west Greenland shelf. WGIW is typically found between ~100–600 m on the west Greenland slope and consists of warm, salty Atlantic-origin water that enters Baffin Bay through eastern Davis Strait as part of the WGC. TrW is the result of mixing between the three water masses just described that enter Baffin Bay and undergo local modification; TrW is typically found at depths >300 m throughout the interior of Baffin Bay.

The northward flowing WGC is the southern source for shallow WGSW and warm subsurface WGIW in Baffin Bay. As these waters flow northward, they transit the ~330 km-wide Davis Strait [Curry et al., 2011, 2014] and eventually reach Uummannaq Trough, one of several cross-shelf troughs that extend across the west Greenland shelf [Ó Cofaigh et al., 2013] (Figure 1b). Uummannaq Trough provides a deep connection between Baffin Bay and the Uummannaq Fjord system, which contains 11 marine-terminating glaciers [Bartholomaus et al., 2016; Rignot et al., 2016a; Felikson et al., 2017]. From the shelf break to Ubekendt Ejland (Figure 1a,b), Uummannaq Trough extends roughly 300 km in the cross-shelf direction, with a mean width of ~62 km and maximum depth of ~800 m [Dowdeswell et al., 2013]. To the east of Ubekendt Ejland, Uummannaq Trough branches northward into the 500–650-m deep Illorsuit Sund before reaching Karrats Isfjord (henceforth referred to as "the Mouth"); here a pair of ~400-m deep sills form a deep connection between Uummannaq Trough and KS and Rink fjords, respectively (Figure 1b,c) [Bartholomaus et al., 2016]. Additionally, the KS Southern Branch contains several ~300 m sills that restrict deep inflow from the south (Figure 1b). Rink is ~5–15 km wide, with maximum basin depth of ~1100 m; the ~4.7 km-wide terminus is grounded at ~850 m [Dowdeswell et al., 2013]. Rink contains a ~650-m deep inner sill located approximately 8 km down-glacier from the terminus (Figure 1c). Located to the south, the shallower KS has a maximum basin depth of ~550 m, with a ~4.2 km-wide terminus grounded at ~250 m [Fried et al., 2015].

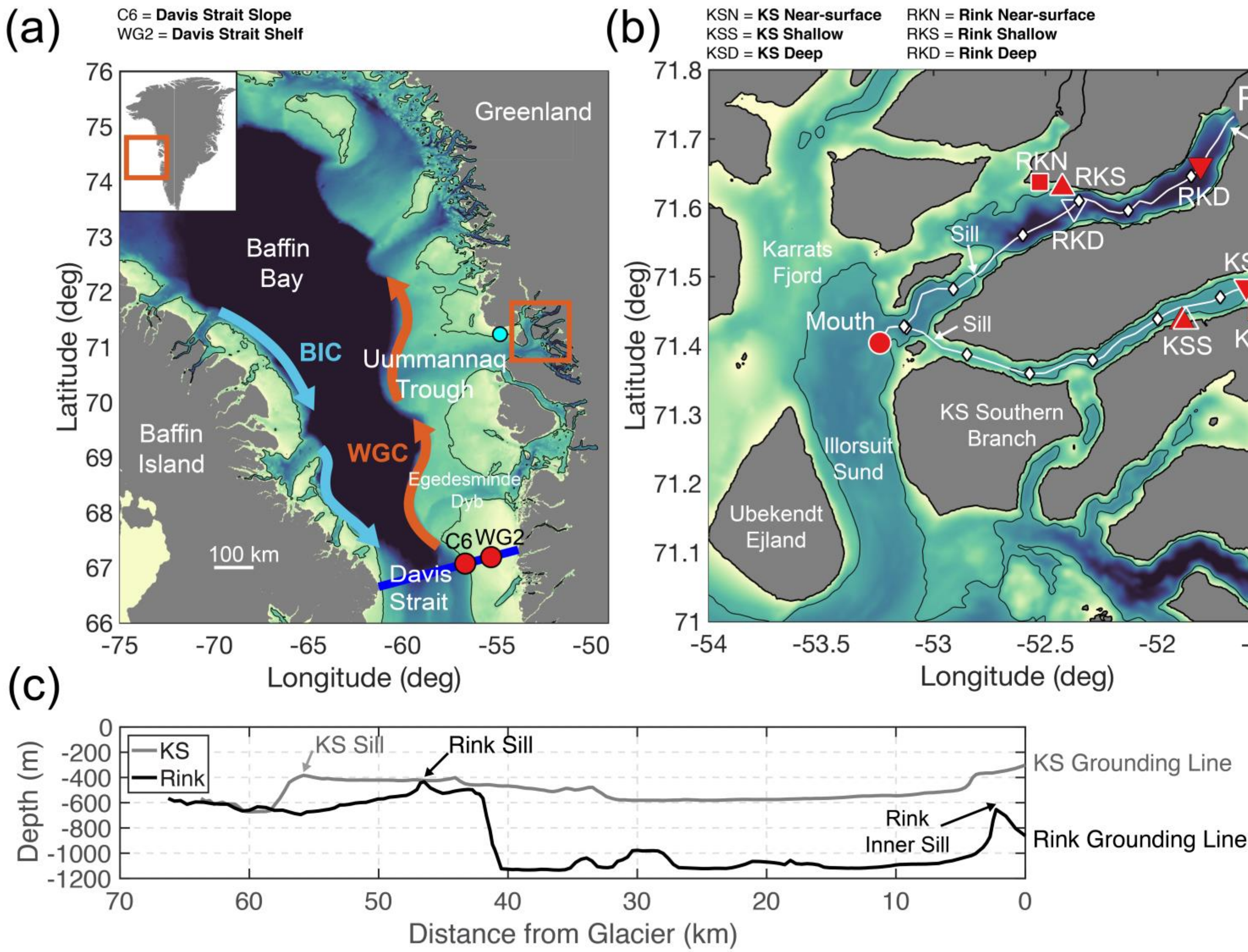

(a)
C6 = Davis Strait Slope
WG2 = Davis Strait Shelf
Greenland
Baffin Bay
BIC
Uummannaq Trough
WGC
Egedesminde Dyb
Baffin Island
100 km
C6
WG2
Davis Strait
Latitude (deg)
Longitude (deg)
(b)
KSN = KS Near-surface
KSS = KS Shallow
KSD = KS Deep
RKN = Rink Near-surface
RKS = Rink Shallow
RKD = Rink Deep
Rink
Inner Sill
RKN
RKS
RKD
Sill
Karrats Fjord
Mouth
KSD
KS
KSS
KSN
KS Southern Branch
Illorsuit Sund
Ubekendt Ejland
Depth (m)
Latitude (deg)
Longitude (deg)
(c)
KS
Rink
KS Sill
Rink Sill
KS Grounding Line
Rink Inner Sill
Rink Grounding Line
Depth (m)
Distance from Glacier (km)

181

Figure 1. Study area and mooring locations. **(a)** Baffin Bay and west Greenland bathymetry. Warm West Greenland Irminger Water (WGIW) flows northward along the continental slope in the West Greenland Current (WGC), while the cold, fresh Baffin Island Current (BIC) flows southward along Baffin Bay toward Davis Strait. Red circles represent Davis Strait moorings; blue line shows transect across Davis Strait. Cyan circle shows location of sea-ice reanalysis near Ubekendt Ejland. **(b)** Fjord mooring locations. Solid red squares, upward-pointing triangles, and downward-pointing triangles represent near-surface, shallow, and deep moorings deployed during 2013 to 2014, respectively. Open white markers show 2014 to 2015 moorings. White lines show KS and Rink thalwegs; white diamonds mark 10 km intervals originating from the termini. Black contour shown in **(a)** and **(b)** is the 450 m isobath. **(c)** Along-thalweg depth for KS (grey line) and Rink (black line). Bathymetric data is from the General Bathymetric Chart of the Ocean (GEBCO) and Morlighem et al. [2017].

2.2 West Greenland Current and Baffin Bay seasonality

The WGSW flows northward year-round, with maximum and minimum velocities reached during September to November and February to April, respectively [Cuny et al., 2005; Curry et al., 2011, 2014]. Warm, fresh WGSW waters arrive in Davis Strait during August to September, with cold, salty waters peaking in April. Seasonality in WGSW temperatures is driven primarily by local atmospheric variability on the west Greenland shelf [Curry et al., 2014], while seasonality in salinity is driven by upstream freshwater transports [de Steur et al., 2017] and buoyancy forcing from terrestrial runoff and glacier, iceberg, and sea-ice melt around Greenland's periphery [Rudels et al., 2002; Sutherland and Pickart, 2008].

Seasonal variability in WGIW transports and hydrography are generally driven by upstream Atlantic-origin water variability in the Labrador [Lilly et al., 2003; Prater, 2002] and Irminger Seas [Spall and Pickart, 2003]. WGIW transports are directed northward, with maxima occurring during October to December and minima reached during June to August. WGIW temperatures at Davis Strait reach maxima during November to December and minima during

July to August, with the seasonal temperature cycle typically ranging from ~2.5–4°C [Curry et al., 2014].

Observations and numerical ocean models [Grist et al., 2014] indicate spatial variability in the seasonal WGIW cycle; this seasonality is reduced and occurs progressively later with increasing northward distance along the west Greenland slope. Additionally, sea-ice cover and wind stress may also contribute to the seasonality of WGIW in Baffin Bay. Sea-ice in Baffin Bay forms during September, with sea-ice cover increasing from north to south during winter months before reaching its maximum extent during March to April [Tang et al., 2004; Dunlap et al., 2007]. From April to August sea-ice cover decreases, with ice-free conditions occurring during September. Strong equatorward winds occur in Baffin Bay during winter, followed by a rapid weakening in spring and reversal toward weak poleward winds during summer.

2.3 Davis Strait data

To investigate hydrographic properties on the west Greenland shelf and slope, we used observations from the Davis Strait mooring array during 2013 to 2015. We limit our analysis to the WG2 and C6 moorings (henceforth referred to as the "Davis Strait Shelf" and "Davis Strait Slope", respectively) located on the shelf and slope at 92- and 570-m depth, respectively (Figure 1a and Table 1) [Curry et al., 2014]. Additionally, we used high-resolution Seaglider surveys and summer conductivity-temperature-depth (CTD) profiles taken at, and north and south of Davis

Strait during 2013 and 2015 (supporting information Figure S1a) to investigate seasonal and spatial variability in WGC properties.

2.4 Fjord data

The following 7 moorings were deployed in the fjords between September 2013 to July 2015 in order to measure water properties (temperature, conductivity, and pressure) throughout the water column (Figure 1b and Table 1).

- Three deep moorings were deployed at the Mouth ("Mouth") and near the maximum depth of the KS ("KS Deep") and Rink basins ("Rink Deep").
- Two shallow moorings were deployed along the KS ("KS Shallow") and Rink ("Rink Shallow") fjord sidewalls.
- Two near-surface moorings were deployed inside shallow embayments in KS ("KS Near-surface") and Rink ("Rink Near-Surface").

All moorings were recovered, serviced, and redeployed during a 20-day cruise in July 2014, resulting in a short data gap. All KS Shallow instruments during 2013 to 2014 were lost shortly after the mooring deployment. Available temperature records span 2013 to 2015, with salinity available at the Mouth during 2013 to 2015 and at KS and Rink during 2014 to 2015. Mooring floats in the upper water column were designed to detach if caught on icebergs, which resulted in the upper section of the Rink Shallow and Rink Deep thermistor chain sinking to depth during both mooring deployments, respectively (Table 1, see footnotes). All subsurface Seabird SBE 56 and SBE 37-SM instruments sampled at 15-minute intervals; near-surface instruments sampled hourly.

Period	Mooring Name	Depth (m)	Location	Instrument / Depth (m)[a]
19 Sept 2013 – 17 Sept 2014	Davis Strait Shelf	92	67.192°N, -55.313°W	SBE 37-SM (20, 76)
19 Sept 2014 – 9 Sept 2015	Davis Strait Shelf	92	67.192°N, -55.313°W	SBE 37-SM (20, 76)
19 Sept 2013 – 10 Sept 2015	Davis Strait Slope	570	67.068°N, -56.681°W	SBE 37-SM (20, 104, 252)[b]
12 Sept 2013 – 24 July 2014	Mouth	536	71.403°N, -53.237°W	SBE 56 (94, 176, 256) SBE 37-SM (53, 337)
16 Sept 2013 – 2 Aug 2014	KS Near-surface	13	71.448°N, -51.559°W	Onset temperature/conductivity/pressure (8, 12.5)[b]
16 Sept 2013 – 28 July 2014	KS Shallow	132	71.434°N, -51.890°W	SBE 56 (82, 92, 102, 112, 122)[b] SBE 37-SM (123)[b]
16 Sept 2013 – 25 July 2014	KS Deep	478	71.485°N, -51.602°W	SBE 56 (136, 156, 176, 196, 216, 236, 256, 276, 296, 316, 336, 356, 410, 440) SBE 37-SM (78, 338)[b]
15 Sept 2013 – 30 July 2014	Rink Near-surface	31	71.636°N, -52.525°W	Onset temperature/conductivity/pressure (25, 30)[b]
17 Sept 2013 – 24 July 2014	Rink Shallow	376	71.629°N, -52.425°W	SBE 56 (99, 109, 119, 129, 139, 149, 164, 179, 199, 219, 239, 284, 309, 334)[b] SBE 37-SM (86, 365)[b]
17 Sept 2013 – 24 July 2014	Rink Deep	1070	71.661°N, -51.808°W	SBE 56 (246/728, 261/778, 276/828, 291/938, 306/968, 321/993, 346/1008, 376/1023, 486/1038, 536/1058, 586/1068, 743, 843, 943) SBE 37-SM (247, 1058.5)[b]
11 Aug 2014 – 11 July 2015	Mouth	535	71.403°N, -53.237°W	SBE 56 (77, 98, 138, 181, 261, 438, 525) SBE 37-SM (54, 342)
9 Aug 2014 – 19 July 2015	KS Near-surface	13.5	71.449°N, -51.554°W	Onset temperature/conductivity/pressure (8, 12.5)[b]
11 Aug 2014 – 11 July 2015	KS Shallow	138	71.434°N, -51.874°W	SBE 56 (74.5, 78, 93, 108) SBE 37-SM (129)
11 Aug 2014 – 11 July 2015	KS Deep	477	71.484°N, -51.603°W	SBE 56 (140, 175, 220, 260, 300, 340, 395, 425) SBE 37-SM (98, 362, *456*)[b]
10 Aug 2014 – 18 July 2015	Rink Near-surface	18	71.637°N, -52.524°W	Onset temperature/conductivity/pressure (11, 17)[b]
11 Aug 2014 – 12 July 2015	Rink Shallow	391	71.629°N, -52.424°W	SBE 56 (117/272, 136/292, 156/312, 176/332, 196/352, 216/372, 256/392, 277, 305.5, 355.5, 411) SBE 37-SM (279)
11 Aug 2014 – 11 July 2015	Rink Deep	1076	71.600°N, -52.371°W	SBE 56 (761, 861, 961) SBE 37-SM (668, 1049)

[a] depths following a forward slash show new depth after float loss
[b] bad/missing data

Table 1: Summary of mooring deployments and instruments. Yellow cells show Davis Strait moorings during 2013 to 2015; blue cells show fjord moorings during 2013 to 2014, and red cells show fjord moorings during 2014 to 2015.

In addition to the mooring data, extensive shipboard CTD surveys were conducted with the *R/V Sanna* at the Mouth and inside KS and Rink during summer 2013, 2014, and 2015 [Bartholomaus et al., 2016; Carroll et al., 2016; Jackson et al., 2017] (supporting information Figure S1b). Fjord CTD profiles were collected with an RBR XR-620. To compare our summer fjord CTD profiles with conditions directly offshore we utilized CTD profiles taken in Uummannaq Trough during a Danish Meteorological Institute (DMI) cruise in June 2013.

2.5 Sea-ice and wind data

To estimate sea-ice cover and wind stress near the Mouth and in Baffin Bay we used the European Centre for Medium-Range Weather Forecasts (ECMWF) ERA-Interim reanalysis product [Dee et al., 2011]. Reanalysis fields were extracted at 6-hour intervals; grid resolution is ~80 km. We neglected all grid cells with > 20% land cover. Sea-ice cover, ranging from a value of 0 to 1, was computed near Illorsuit Sund (71.2278°N, -54.8437°W; Figure 1a, cyan circle) and averaged over Baffin Bay (65 to 76°N and -75 to -50°W) (supporting information Figure S2).

3 Results

3.1 Water Masses

We first present potential temperature-salinity (θ-S) diagrams showing all summer CTD profiles and mooring data used in this study. For additional details on mooring and CTD locations see Figure 1b and supporting information Figure S1, respectively. The general θ-S structure consists of a thick layer of warm, salty Atlantic-origin water overlain by a cold, fresh layer of Polar-origin water and thin layer of warm, fresh surface water. The warmest, saltiest WGIW during summer months was found near Davis Strait (Figure 2a, orange lines), with deep temperatures reaching ~6°C. Fjord and Uummannaq Trough WGIW was generally cooler than Davis Strait, with deep summer fjord θ-S converging to ~3°C and ~34.6, respectively. TrW and AW in the fjords was warmer compared to Davis Strait and Uummannaq Trough, often by several degrees; here θ-S properties were pulled upwards toward mixing lines with subglacial discharge (Figure 2a, magenta lines), indicating the presence of glacially-modified waters at mid-column depth. We note that fjord TrW and AW θ-S properties varied considerably from fjord to fjord, with the warmest mid-column temperatures found in Rink, followed by the Mouth and KS. Near the surface, WGSW in the fjords was cooler and fresher than Davis Strait and Uummannaq Trough. Fjord mooring WGIW and TrW θ-S properties generally followed a mixing line with cooler, fresher AW (Figure 2b), with the warmest annual WGIW found at the Mouth (Figure 2b, red circles). At near-surface depths, fjord mooring θ-S properties spanned temperatures near the in-situ freezing point up to ~3.5°C

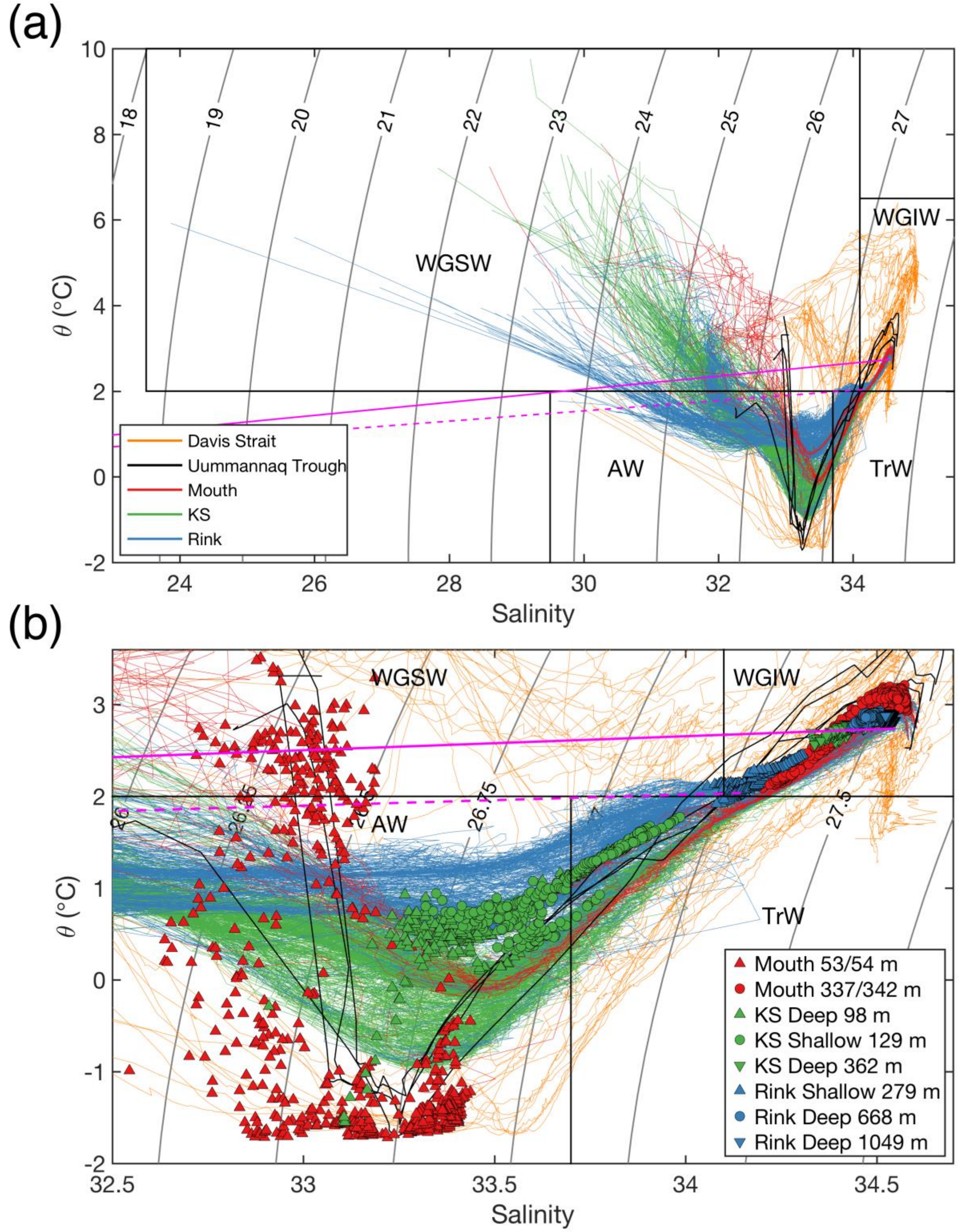

Figure 2: **(a)** Potential temperature-salinity diagram for all summer CTD profiles (lines) and **(b)** mooring data (markers) where salinity data is available. Grey contours in **(a)** and **(b)** represent isopycnals spaced at 1 and 0.25 kg m^{-3} intervals, respectively. Dashed and solid magenta lines

show mixing lines for subglacial discharge with mean water properties at the KS and Rink grounding line depth (250 and 850 m), respectively. Baffin Bay water masses defined in Curry et al. [2014] are outlined in black boxes. For CTD locations see supporting information Figure S1.

3.2 Fjord temperature summary

We next summarize fjord temperature trends from 2013 to 2015, in the context of sea-ice cover and wind stress (Figure 3). During 2013 to 2015, mean sea-ice cover in Baffin Bay began to increase in late October, with values above 0.75 sustained from December to May (Figure 3a). Near Illorsuit Sund (Figure 1a, cyan circle), sea-ice formation began later in the season during January to February, with a shorter duration of seasonal sea-ice cover (Figure 3a, black line). For both years, mean wind stresses in Baffin Bay were generally oriented equatorward (upwelling-favorable conditions) during fall and winter, with peak wind stresses occurring during November to January (Figure 3b). During summer, wind stresses were weaker and typically oriented poleward.

Fjord temperatures above the sill depth exhibited a clear seasonal cycle, with a cooling of waters in the upper ~150 m and lifting of isotherms below 150 m during winter and spring (Figure 3c-e). Here we use the 2.86°C isotherm as an indicator of waters that are initially near, or slightly below the sill depth (Figure 3c-e, black contours). During both years, Mouth isotherms below ~250 m-depth began to shoal during December to January, with the 2.86°C isotherm (that was initially near sill depth) reaching a minimum depth of ~250 m during April to May (Figure 3c). At KS during 2013 to 2014, the 2.86°C isotherm shoaled above the sill (black horizontal dashed line) during March, reaching a minimum depth of ~340 m during May; this was followed by a return to the sill depth by mid-summer (Figure 3d). During 2014 to 2015, the 2.86°C isotherm reached a shallower depth of ~290 m and remained above the sill during summer. Below the sill depth in Rink, temperatures generally cooled during fall (Figure 3e), with synoptic warming events occurring from winter to spring. During 2013 to 2014, the Rink basin 2.86°C isotherm shoaled from near-bottom depth to ~730 m during mid-March to April. In the following year, the 2.86°C isotherm gradually deepened from July to December, followed by a rapid shoaling during January.

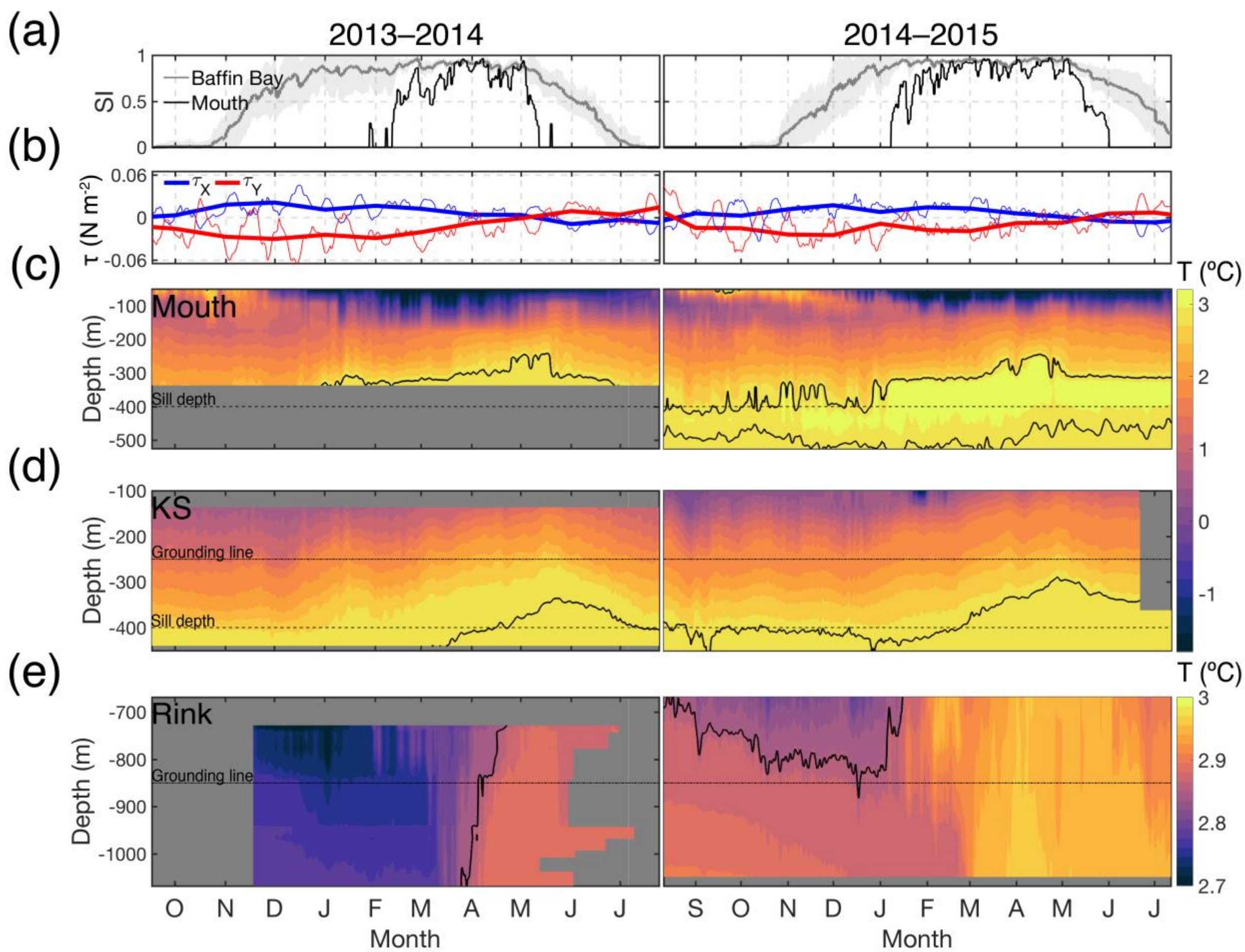

Figure 3. (a) Summary plot of sea-ice cover, **(b)** Baffin Bay wind stress, and fjord temperature from 2013 to 2015 at the **(c)** Mouth, **(d)** KS, and **(e)** Rink basin. Grey line in **(a)** shows sea-ice cover averaged over the Baffin Bay box, shaded error bars show two standard deviations from the mean; black line shows sea-ice cover near the Mouth. Wind stress shown in **(b)** is averaged over Baffin Bay; thick lines represent monthly averages; thin lines are 6-hour values smoothed with a 7-day running mean. Solid black line in **(c-d)** represents the 2.86°C isotherm. Horizontal

black dashed line in **(c)** and **(d)** shows the sill depth; black dot-dashed line in **(d)** and **(e)** shows the grounding line depth.

3.3 Layer 1 variability (L1, 0–100 m)

Having shown a summary of the fjord temperature record, we next define three vertical layers for Davis Strait and fjord waters: Layer 1 (L1, 0–100 m) is from the surface to below the mixed layer, Layer 2 (L2, 100–400 m) is located from below the mixed layer depth to the sill depth, and Layer 3 (L3, 400 m to maximum fjord depth) is below the sill depth.

L1 temperatures at the West Greenland Shelf and fjords evolved seasonally (Figure 4c), with the fjords generally exhibiting shorter periods of seasonal warming. For both years examined, West Greenland Shelf temperatures at 20- and 76-m depth began to warm in March, reaching maximum temperatures of 4.5–5°C between August to September. After reaching seasonal maxima, temperatures at both depths began to cool concurrently, with temperatures at 20-m depth reaching seasonal minima slightly above the in-situ freezing point during winter. Compared to the West Greenland Shelf, L1 fjord temperatures were generally ~1–1.5°C cooler during summer and fall and exhibited slower rates of warming during spring and early summer. For both years, peak Mouth temperatures at 54-m depth were ~1–1.5°C cooler than the West Greenland Shelf at 20- and 76-m depth, with comparable temperatures during fall. L1 salinities at the West Greenland Shelf and Mouth tended to increase in concert during early winter; salinity maxima were reached at the Mouth during May to July, slightly before the West Greenland Shelf (Figure 4d). During late summer, salinities at the West Greenland Shelf and Mouth began to decrease, with minima reached during winter. During fall 2013 and 2014, Mouth waters at 54-m depth were generally more saline than Davis Strait Shelf waters at 20- and 76-m depth.

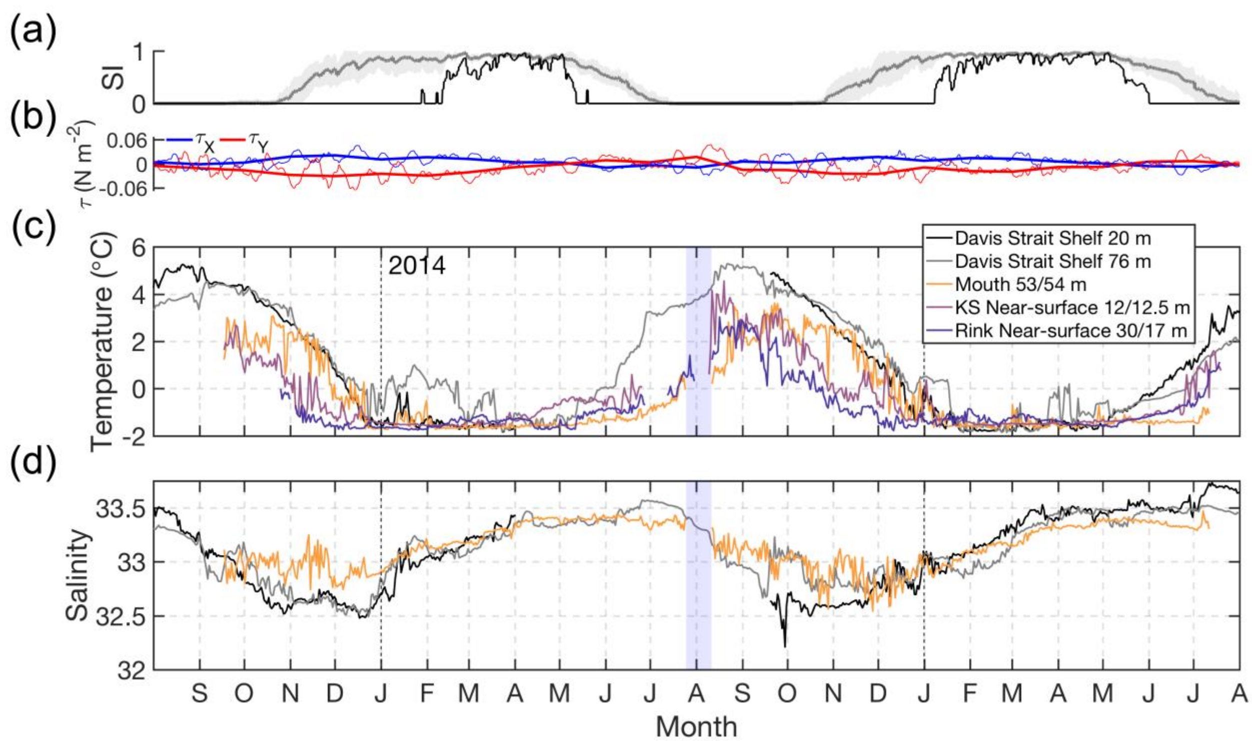

Figure 4. Time series of **(a)** sea-ice cover, **(b)** Baffin Bay wind stress, and Layer 1 (L1, 0–100 m) **(c)** temperature and **(d)** salinity at the Davis Strait Shelf, Mouth, and KS and Rink during 2013 to 2015. Grey line in **(a)** shows sea-ice cover averaged over the Baffin Bay box, shaded error bars show two standard deviations from the mean; black line shows sea-ice cover near the Mouth. Wind stress shown in **(b)** is averaged over the Baffin Bay box. Thick lines represent monthly averages; thin lines are 6-hour values smoothed with a 7-day running mean. Vertical dashed black lines in **(c)** and **(d)** indicate the start of each year; blue shaded region shows data gap from mooring redeployment. Note that KS and Rink instrument depths varied slightly between mooring deployments (as shown in the legend).

3.4 Layer 2 variability (L2, 100–400 m)

L2 temperatures at the Mouth, KS, and Rink demonstrate that the seasonal fjord temperature cycle exhibits considerable lag compared to Davis Strait Slope waters (Figure 5c,d). Davis Strait Slope temperatures at 252-m depth reached annual minima of 1.76 and 2.72°C during July 2013 and August 2014, respectively. Starting in late August, temperatures began to rise steadily, albeit with some high-frequency cooling events during fall. Maximum annual temperatures of 5.96 and 6.17°C were reached during December 2013 and 2014, respectively. Peak temperatures during both years cooled by ~1°C between late December to February, before plateauing and then slightly cooling from February to August.

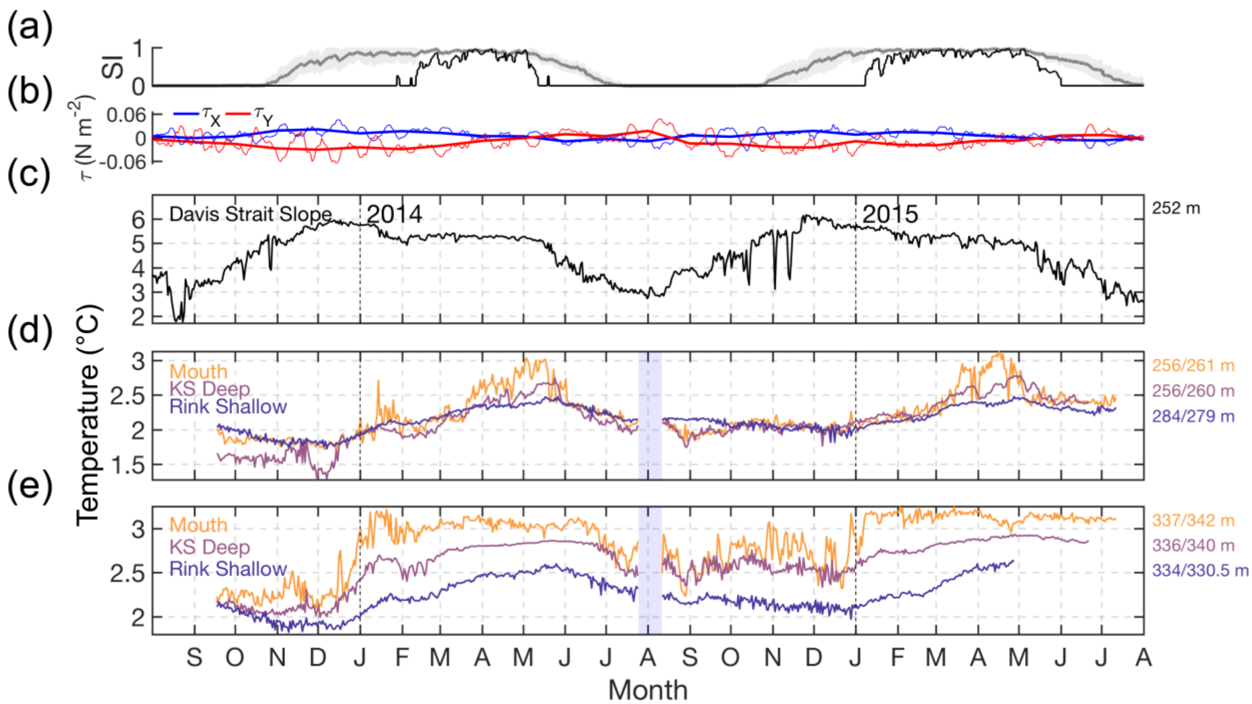

Figure 5. Daily time series of **(a)** sea-ice cover, **(b)** Baffin Bay wind stress, and Layer 2 (L2, 100–400 m) temperature at **(c)** the Davis Strait Slope and **(d,e)** Mouth, KS, and Rink during 2013 to 2015. Grey line in **(a)** shows sea-ice cover averaged over the Baffin Bay box, shaded error bars show two standard deviations from the mean; black line shows sea-ice cover near the Mouth. Wind stress shown in **(b)** is averaged over the Baffin Bay box. Thick lines represent monthly averages; thin lines are 6-hour values smoothed with a 7-day running mean. Vertical dashed black lines in **(c-e)** indicate the start of each year; blue shaded region shows data gap from mooring redeployment. Note that KS and Rink instrument depths varied slightly between mooring deployments (as shown to the right of panels **(d)** and **(e)**).

Mouth, KS, and Rink temperatures between 256–284 m were generally several degrees cooler and lagged West Greenland Slope waters by ~5–6 months (Figure 5d). Fjord temperatures within this depth range warmed from December to June, with maximum annual temperatures being ~3–3.5°C cooler than the Davis Strait Slope. Deeper in the water column between 337–342 m, the Mouth generally had the warmest temperatures year-round compared to KS and Rink (Figure 5e). Within this depth range, Mouth temperatures rapidly warmed by ~1.1°C from mid-December to mid-January. Maximum 2014 and 2015 Mouth temperatures occurred in January and early March, respectively; these maxima were followed by relatively uniform temperatures during late-winter to spring and cooling during summer. The seasonal temperature cycle at KS and Rink exhibited a more gradual warming period that remained active until May to June. Inside KS and Rink, temperatures were generally cooler than the Mouth.

Examination of L2 θ-S properties at the Mouth shows the arrival of warm, dense waters during winter and spring, followed by a cooling and freshening period from mid-summer to fall (Figure 6a,b). At the Mouth, the majority of warming occurred during a relatively short period spanning December to January; here θ-S properties transitioned along a mixing line with warmer, saltier WGIW. For both years, the densest waters arrived at the Mouth during late spring, resulting in a deviation in θ-S properties from the seasonal mixing line. During mid-summer to fall, Mouth waters cooled and freshened, generally retracing the seasonal mixing line. During 2014 to 2015, the seasonal warming cycle at KS (362 m) lagged the Mouth, with the warmest, densest waters arriving during May to June (Figure 6c, black outlined region); peak KS θ-S during these months was generally cooler and fresher compared to spring properties at the Mouth. At shallower depth in Rink (279 m), the warmest, densest waters arrived earlier during spring, with winter and spring θ-S properties falling along a mixing line that had a reduced slope compared to the seasonal mixing line at the Mouth.

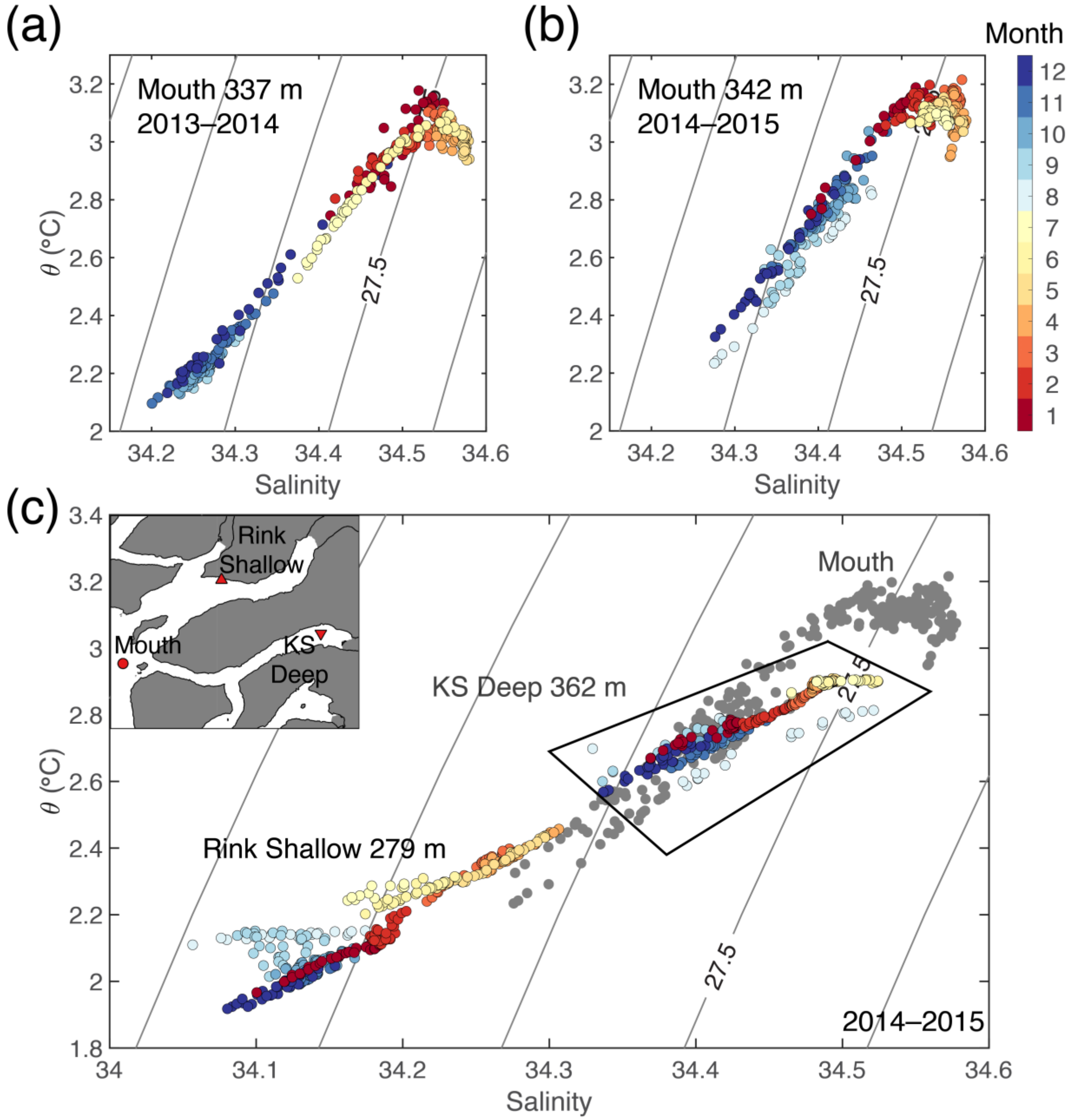

Figure 6. Layer 2 (L2, 100–400 m) potential temperature-salinity diagrams for **(a,b)** the Mouth during 2013 to 2015 and **(c)** KS and Rink during 2014 to 2015. Temperature and salinity are averaged daily; colors show month. Grey contours represent isopycnals spaced at 0.1 kg m^{-3} intervals. Gray circles in **(c)** represent Mouth θ-S from **(b)**, shown for comparison. Black

outlined region in **(c)** is KS Deep at 362-m depth; all other colored circles are Rink Shallow at 279-m depth. Inset shows mooring locations.

3.5 Layer 3 variability (L3, 400 m to maximum fjord depth)

KS and Rink L3 waters experienced cooling from late-summer to winter, followed by the inflow of warm, weakly-stratified waters during winter and spring (Figure 7a,b). During September to December 2013, KS L3 temperatures at 440-m depth exhibited a gradual cooling cycle, reaching an annual minimum in December. During both years, KS near-bottom waters warmed at relatively constant rates from late-December to mid-April, followed by sharp summer warming events that peaked in June. In Rink, L3 waters cooled and freshened during fall (Figure 7b,c), with the strongest vertical temperature stratification occurring during December, immediately before the shallowest sensor began to show warming. The 2014 (2015) warming at Rink near-bottom depth, which occurred during March (February), lagged the arrival of warm waters at the shallowest L3 Rink thermistor by roughly 84 (64) days. Vertical temperature stratification decreased as warm waters arrived at progressively deeper depths in Rink, with L3 temperatures being almost homogenous during April to May. Rink L3 near-bottom temperatures reached annual maxima of 2.91 and 2.99°C during May 2014 and April 2015, respectively. In

June 2015, Rink L3 temperatures began to restratify and cool; this feature was less pronounced in 2014.

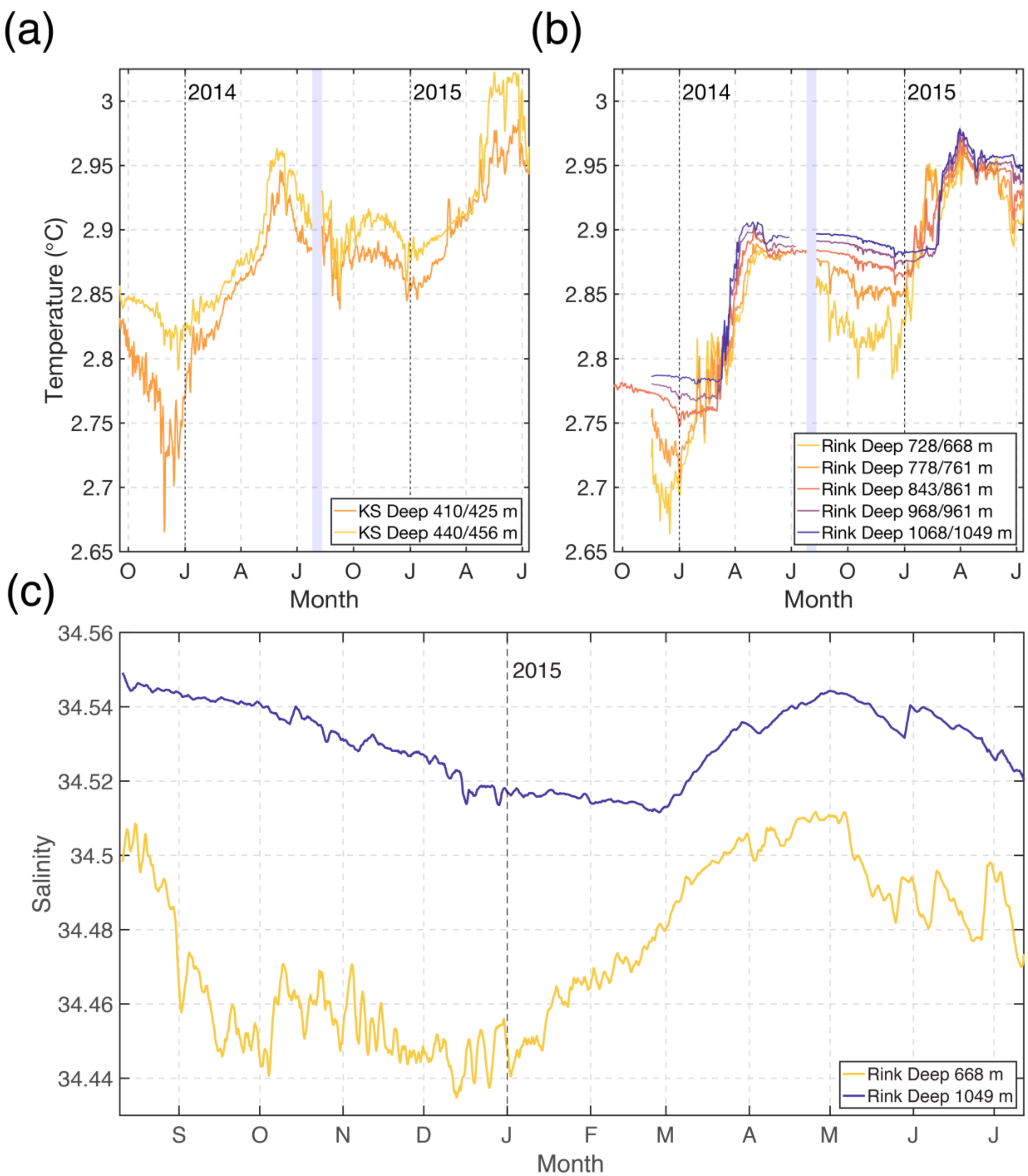

Figure 7. Time series of Layer 3 (L3, 400 m to maximum fjord depth) temperature in **(a)** KS and **(b)** Rink during 2013 to 2015. **(c)** L3 salinity in Rink during 2014 to 2015. Temperature and salinity are low-pass filtered with 50-hour, forward-running mean. Vertical dashed black lines indicate the start of each year. Note that instrument depths in KS and Rink varied slightly between mooring deployments (as shown in the legends).

The arrival of warm, dense waters in the Rink basin generally occurred when L2 potential densities at the mouth exceeded that of L3 in Rink (Figure 8a, red markers). From summer to early-winter, Rink θ-S properties at 668-m depth evolved along a mixing line with cooler, fresher waters (Figure 8a, blue markers). Once positive density differences between L2 Mouth waters and L3 Rink waters at 668-m depth were sustained (Figure 8b, shaded yellow region), Rink potential temperature and salinity at 668-m depth began to increase in concert. Deeper in the water column at 1049-m depth, Rink θ-S gradually cooled and freshened from August to March, exhibiting less variance in θ-S compared to 668 m. Rink salinity at 1049-m depth generally increased from March to May, when L2 Mouth waters were denser (Figure 8b, shaded purple region); temperatures reached maxima during April and then began to cool slightly while salinity continued to increase. From May to July, Rink waters at 1049-m depth generally freshened and cooled, coinciding with a decrease in L2 density at the Mouth.

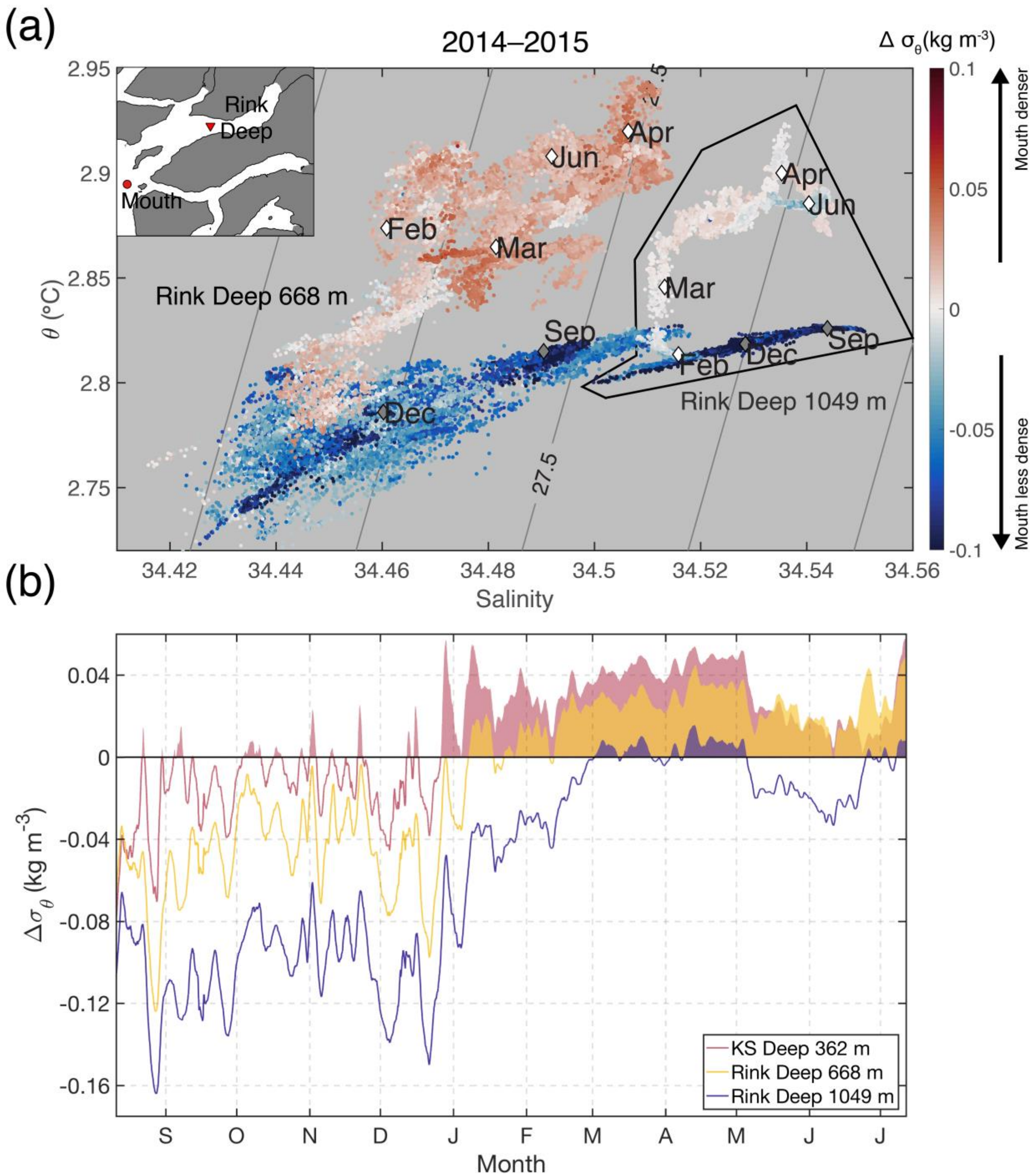

Figure 8. (a) Layer 3 (L3, 400 m to maximum fjord depth) potential temperature-salinity diagram for Rink during 2014 to 2015. Black outlined region is 1049-m depth; all other colored circles are 668-m depth. Colors show the potential density difference between the Mouth (342 m) and Rink Deep at 668 and 1049 m, respectively. Diamonds show θ-S on the first day of selected months; grey diamonds show 2014 months and white diamonds represent 2015. Grey contours represent isopycnals spaced at 0.025 kg m^{-3} intervals and inset shows mooring locations. **(b)** Time series of potential density difference between L2 waters at the Mouth (342 m) and L3 waters in Rink during 2014 to 2015. Potential density is low-pass filtered with 50-hour, forward-running mean; shaded regions show when L2 Mouth density exceeds that of the fjords. Note that the potential density difference between the Mouth and the deepest KS SBE 37-SM (362 m) is shown for comparison (red line and shaded region).

4 Discussion

4.1 Renewal of fjord waters

Our results demonstrate the clear seasonal cycle in L1 and L2 hydrography at the Mouth, KS, and Rink. These observations provide a striking contrast to previous observations from Sermilik and Kangerdlugssuaq fjords in southeast Greenland [Jackson et al., 2014; Straneo et al., 2016], where variance in mid-column hydrography during non-summer months is dominated by strong synoptic-scale variability. Below the sill, fjord renewal typically occurs when waters at the sill are dense enough to replace deep basin waters [Edwards and Edelsten, 1976]. After renewal events, turbulent diffusion gradually reduces the density of basin waters, preconditioning the basin for subsequent renewal [Skreslet and Loeng, 1977]. We find that the sub-annual renewal of L3 fjord waters was initiated when dense L2 waters arrived at the Mouth during December to January, potentially indicating the inflow of warm, salty WGIW into the KS and Rink basins (Figures 7 and 8). At 1049-m depth in Rink, renewal occurred intermittently and over shorter durations, suggesting that basin waters below the ~850-m deep glacier were only partially renewed.

This sub-annual mode of basin renewal is similar to moored observations from Ilulissat Icefjord, west Greenland (69°N) [Gladish et al., 2015a,b], where dense coastal inflows associated with rising coastal isopycnals cascade over the ~250-m deep sill from winter to spring. Dense coastal inflows in Godthåbsfjord, located south of Davis Strait at 64°N, are generally more episodic [Mortensen et al., 2011]. In Godthåbsfjord, warm (> 2°C) and cold (< 2°C) inflows, typically last ~1–3 months and are the primary cause of basin water variability from December to June.

We note that the complex, interconnected network of basins and sills in the Uummannaq Fjord system [Rignot et al., 2016a] suggests that renewal may be dependent on the preconditioning of basin waters during late-summer and fall (Figure 7c and Figure 8). The reduction of below-sill density due to vertical turbulent diffusion and enhanced mixing from terminus melt [Beaird et al., 2015], deep-keeled iceberg melt [Moon et al., 2017], and subglacial discharge plumes [Carroll et al., 2015] could act to precondition fjord basins for winter and spring renewal events. For Rink, the cooling observed from early to mid-October 2014 (Figure 7b) represents roughly 9.8×10^4 J m^{-2} of heat loss in the lower 288 m of the water column. This cooling rate is consistent with an average turbulent diffusivity of ~10^{-4} m^2 s^{-1} at 761 m depth based on a 1-dimensional heat balance between the tendency and vertical mixing. We note that additional fjord-scale processes and elevated turbulent mixing resulting from hydraulics and ocean-ice interactions may be critical for preconditioning renewal of fjord bottom waters. For fjords with large vertical eddy diffusivities, the density at, or outside of the sill could remain constant throughout the year, with sub-annual renewal of basin waters induced by turbulent mixing alone.

By mid-summer, the effect of the sill in separating dense Mouth waters and lighter basin waters is most pronounced in Rink (supporting information Figure S3, blue markers). In shallower KS, basin water densities are similar to the Mouth (supporting information Figure S3, green markers), implying a more complete renewal of the smaller KS basin volume by mid-summer. Interestingly, the KS Southern Branch contains the lightest water in the fjord (supporting information Figure S3, magenta markers); this may result from increased mixing or topographic blocking of dense coastal inflows by the series of ~300-m deep sills located along the KS Southern Branch. In summary, our observations suggest that dense coastal inflows are important mechanisms for basin water renewal in west Greenland during non-summer months and may be strongly regulated by local bathymetric features (e.g., sills, basin depth, and fjord volume) [Rignot et al., 2016a; Fenty et al., 2016].

4.2 Remote forcing

For both years examined, peak L2 temperatures at the Davis Strait Slope occurred in December (Figure 5c), with warm, dense waters arriving at equivalent depths in the Mouth ~5–6 months later during April to May (Figure 5d). To investigate the feasibility that these dense fjord waters originated from Davis Strait, we first examine summer CTD profiles that span the potential advective pathway of WGIW from south of Davis Strait to the Mouth (Figure 9 and supporting information Figure S1a). Across this ~7.5° latitudinal gradient, we find that deep θ-S properties are concentrated near the 27.6 kg m^{-3} isopycnal, suggestive of a common deep source of WGIW. During summer, the warmest (~5°C), densest waters are found south of Davis Strait (Figure 9, orange circles) in the northern Labrador Sea. Moving northward, θ-S properties progressively cool and freshen at, and to the north of Davis Strait (purple and blue circles); this may be due in part to eddy-driven mixing along the west Greenland slope [Lilly et al., 2003; Kawasaki and Hasumi, 2014] and strong shear and recirculation in eastern Davis Strait [Dunlap and Tang, 2006]. Deep Mouth θ-S properties are similar to waters found north of Davis Strait (orange circles) and directly offshore in Uummannaq Trough (Figure 9a, grey circles). Examination of repeated Seaglider profiles from Davis Strait during 2013 and 2014 to 2015 (Figure 9a,b, magenta markers) shows a strong seasonal cycle in deep WGIW θ-S properties, with peak temperatures occurring during December. For both years, Seaglider sections taken across Davis Strait (Figure 9c and supporting information Figure S3) reveal a thickening and warming of WGIW core waters during fall and winter.

Having shown that a common source of deep WGIW is present along the west Greenland slope and in Uummannaq Trough, we next estimate the advective timescale for L2 waters to transit from Davis Strait to the Mouth. Assuming a characteristic velocity of ~0.05 m s^{-1} in the subsurface WGC north of Davis Strait [Dunlap and Tang, 2006] and an along-isobath length scale of ~700 km between Davis Strait and the Mouth yields an advective timescale of ~5 months. This estimate is in reasonable agreement with the observed lag between peak L2 temperatures within 256–284 m at the Davis Strait Slope and Mouth (Figure 5c) and numerical drifter simulations from Grist et al. [2014]. However, we acknowledge that these advective timescales cannot explain the rapid temperature and salinity increase observed at the Mouth at ~340-m depth during December to January (Figure 5e), suggesting that this warming event may result in part from local forcing and not merely an advective signal from Davis Strait.

4.3 Local offshore forcing

Observations and ocean model results from [Grist et al. 2014] show that the seasonal cycle in WGIW temperatures at 300-m depth along the west Greenland slope is 1) reduced to the north of 70°N but 2) more pronounced than at 400-m depth. The latter observation suggests that in addition to the advection of WGIW from the Irminger Basin, there could be a local surface influence on the seasonal cycle. To explore local surface mechanisms for cross-shelf exchange, we utilize monthly-averaged reanalysis of sea-ice cover and wind stress in Baffin Bay (supporting information Figure S2). We find that the rapid Mouth temperature and salinity increase at ~340-m depth during December to January coincides with strong upwelling-favorable wind stress, combined with relatively ice-free conditions outside Uummannaq Bay. We speculate that offshore Ekman transport results in upwelling of WGIW along Uummannaq Trough [Ribergaard et al., 2004], with the interaction between upwelling dynamics and near-shore bathymetry [Klink, 1996; She and Klink, 2000] resulting in an intrusion of WGIW into Illorsuit Sund (Figure 1b). After rigid sea-ice forms in Uummannaq Bay and upwelling-favorable winds relax, these dense waters may remain confined in the Illorsuit Sund basin, which could explain the relatively constant temperatures observed at ~340-m depth in the Mouth from spring to early summer (Figure 5e). In summary, we anticipate that the arrival of warm, dense waters at ~340-m depth in the Mouth result from both northward advection of seasonality in the WGC and cross-shelf exchange processes driven by localized changes in surface boundary conditions.

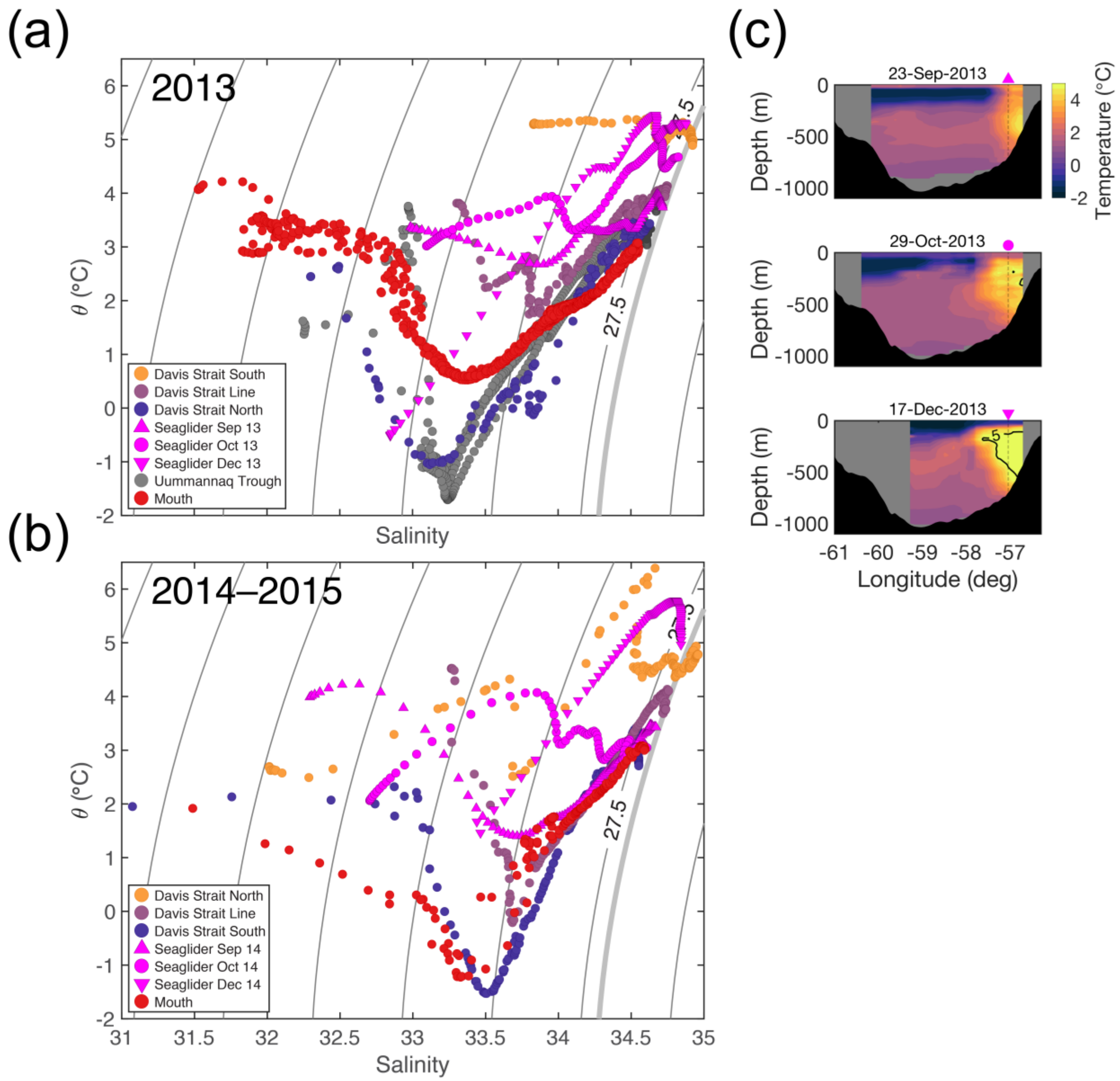

Figure 9. Potential temperature-salinity diagram showing September CTD profiles spanning south of Davis Strait to the Mouth and Seaglider profiles taken on the Davis Strait slope during **(a)** 2013 and **(b)** 2014 to 2015. For all profiles, the maximum depth shown is 400 m (fjord sill depth). Grey contours represent isopycnals spaced at 0.5 kg m^{-3} intervals; thick grey contour shows the 27.6 kg m^{-3} isopycnal. **(c)** Seaglider temperature sections from Davis Strait during

2013, magenta markers and dashed vertical black lines show the Seaglider profiles used in **(a)**. Black contour is the 5°C isotherm.

4.4 Comparison to other Greenland fjords

In order to parameterize how fjords modulate the mixing of coastal and glacially-modified waters in climate models, which do not explicitly resolve fjords at the spatial scales described here, it is necessary to first characterize the relative magnitude and timing of fjord-scale processes (i.e., estuarine and subglacial discharge-driven circulation, intermediary circulation, and dense coastal inflows) in various Greenland fjords. To first order, we expect these fjord-scale processes to be controlled by fjord-glacier geometry [Carroll et al., 2016, 2017], seasonality in offshore boundary conditions [Christoffersen et al., 2011; Sutherland et al., 2013; Harden et al., 2014], along-shelf [Jackson et al., 2014] and along-fjord wind forcing [Oltmanns et al., 2014], and bathymetric constrictions in the trough-shelf-fjord system.

For the fjords examined in this study, the strong seasonal cycle observed in L2 waters may result from a combination of 1) the open connection to the WGC provided by Uummannaq Trough, 2) the lack of barrier wind dynamics in Baffin Bay, and 3) local air-sea forcing. In southeast Greenland, strong low-pressure systems are constrained against steep coastal topography, resulting in strong along-shelf barrier winds [Harden et al., 2011, 2012]. For fjords such as Sermilik and Kangerdlugssuaq, exposure to frequent barrier winds and lack of shallow sills [Sutherland et al., 2014] result in highly dynamic systems, where hydrographic properties respond rapidly to changes in adjacent coastal waters [Straneo et al., 2010; Harden et al., 2014]. Winter wind velocities computed from reanalysis near Ubekendt Ejland (Figure 1, cyan circle) rarely exceed 15 m s^{-1} (not shown), suggesting that the Uummannaq Fjord system is exposed to weaker shelf winds compared to systems in southeast Greenland. We note that seasonality is also observed in Sermilik Fjord [Straneo et al., 2016]; however, it is often masked by strong synoptic-scale variability and limited to depths above ~300–400 m. This may be due in part to the relatively open connection at the fjord mouth and ~400 m deep sill near the shelf break of the Irminger Sea [Sutherland et al., 2013]. For Kangerdlugssuaq, ocean reanalysis of offshore water properties suggests that Atlantic-origin water intrudes into the cross-shelf trough during spring to summer [Christoffersen et al., 2011], with both estuarine and subglacial discharge-driven circulation [Inall et al., 2014] and intermediary [Sutherland et al., 2014] circulation active inside the fjord. For fjords with shallow sills, such as Godthåbsfjord and Ilulissat Icefjord, we would expect shelf-forced intermediary and katabatic wind-driven circulation to be arrested [Spall et al., 2017], with hydrographic variability during non-summer months driven by tidal mixing and dense coastal inflows [Mortensen at., 2014; Gladish et al., 2015a]. We note that compared to KS and Rink, seasonal inflow of the warmest WGIW waters into Ilulissat Icefjord is restricted offshore by the ~300-m deep Egedesminde Dyb sill (Figure 1a); here roughly equal parts of WGIW and AW fill the fjord basin during spring to summer [Gladish et al., 2015b].

In summary, these results highlight the importance of sub-annual and seasonal fjord-scale processes and submarine topography (i.e., troughs, basins, and sills) in determining whether warm Atlantic-origin waters reach individual glacier termini [Fenty et al., 2017]. We stress that large interannual signals that propagate around the subpolar North Atlantic gyre [Flatau et al., 2003; Hakkinen and Rhines, 2004] must transit cross-shelf troughs, fjords, and sills if they are to affect Greenland outlet glaciers [Holland et al., 2008], and hence ice sheet dynamics.

5 Summary and Conclusions

We use a two-year hydrographic record from a suite of moorings in Davis Strait and two neighboring west Greenland fjords with contrasting fjord and glacier geometry to characterize sub-annual and seasonal variability of shelf and fjord water properties. In both fjords, hydrographic variability above the sill exhibits a clear seasonal cycle, with peak subsurface temperatures occurring during spring to summer. Below the ~400-m deep sill, renewal of basin waters coincides with the arrival of dense Atlantic-origin waters at the fjord mouth. These results contrast previous observations from southeast Greenland, where variability during non-summer months is dominated by strong synoptic-scale variability. We then use Seaglider and CTD observations from Davis Strait, along with reanalysis of sea-ice cover and wind stress in Baffin Bay, to explore the role of seasonality in the West Greenland Current and local air-sea forcing in driving fjord renewal. Our results highlight the important role of submarine topography and local cross-shelf exchange in connecting small-scale fjords with the large-scale Greenland boundary current. This work demonstrates that sustained monitoring of the Greenland shelf and fjords is required to understand interannual warming and freshening trends, as synoptic summer observations can alias sub-annual and seasonal variability. Future observational and modeling efforts that focus on understanding how water properties are modified during the transit from the shelf to ice sheet are critical.

Acknowledgments and Data

This work was partially supported by the National Aeronautics and Space Administration

Grant NNX12AP50G and the U.S. National Science Foundation Grant PLR-1504521. J.P Grist was funded by 'The North Atlantic Climate System Integrated Study: ACSIS', programme (NE/N018044/1) of the Natural Environment Research Council of the UK. The 2014 *R/V Sanna* cruise received funding from EUROFLEETS2, a European Community - Research Infrastructure Action under the FP7 "Capacities" Specific Programme. Grant agreement n.14/1211168/B ORCA. All mooring data is available for download through NOAA National Centers for Environmental Information (NCEI) at http://accession.nodc.noaa.gov/0173969. We would like to thank three anonymous reviewers and the editor for their thoughtful and constructive criticism of this work.

References

Aure, J., and Stigebrandt, A. (1990). Quantitative estimates of the eutrophication effects of fish farming on fjords. Aquaculture, 90(2), 135–156.

Aure, J., Molvær, J., and Stigebrandt, A. (1996). Observations of inshore water exchange forced by a fluctuating offshore density field. Marine Pollution Bulletin, 33(1), 112–119.

Bartholomaus, T. C., Stearns, L. A., Sutherland, D. A., Shroyer, E. L., Nash, J. D., Walker, R. T., Catania, G. A., Felikson, D., Carroll, D., Fried, M. J., and Noël, B. P. Y. (2016). Contrasts in the response of adjacent fjords and glaciers to ice-sheet surface melt in West Greenland. Annals of Glaciology, 57(73), 25–38.

Beaird, N., Straneo, F., and Jenkins, W. (2015), Spreading of Greenland meltwaters in the ocean revealed by noble gases. Geophysical Research Letters, 42, 7705–7713.

Boone, W., Rysgaard, S., Carlson, D. F., Meire, L., Kirillov, S., Mortensen, J., Dmitrenko, I. Vergeynst, L., and Sejr, M. K. (2018). Coastal freshening prevents fjord bottom water renewal in Northeast Greenland: A mooring study from 2003 to 2015. Geophysical Research Letters, 45, https://doi.org/10.1002/2017GL076591

Carroll, D., Sutherland, D. A., Shroyer, E. L., Nash, J. D., Catania, G. A., and Stearns, L. A. (2015). Modeling turbulent subglacial meltwater plumes: Implications for fjord-scale buoyancy-driven circulation. Journal of Physical Oceanography, 45(8), 2169–2185.

Carroll, D., Sutherland, D. A., Hudson, B., Moon, T., Catania, G. A., Shroyer, E. L., Nash, J. D., Bartholomaus, T. C., Felikson, D., Stearns, L. A., and Noël, B. P. Y. (2016). The impact of glacier geometry on meltwater plume structure and submarine melt in Greenland fjords. Geophysical Research Letters, 43(18), 9739–9748.

Carroll, D., Sutherland, D. A., Shroyer, E. L., Nash, J. D., Catania, G. A., and Stearns, L. A. (2017). Subglacial discharge-driven renewal of tidewater glacier fjords. Journal of Geophysical Research: Oceans, 122, 6611–6629.

Cofaigh, C. Ó., Dowdeswell, J. A., Jennings, A. E., Hogan, K. A., Kilfeather, A., Hiemstra, J. F., Noormets, R., Evans, J., McCarthy, D. J., Andrews, J. T., and Lloyd, J. M. (2013). An extensive and dynamic ice sheet on the West Greenland shelf during the last glacial cycle. Geology, 41(2), 219–222.

Cowton, T., Slater, D., Sole, A., Goldberg, D., and Nienow, P. (2015). Modeling the impact of glacial runoff on fjord circulation and submarine melt rate using a new subgrid-scale parameterization for glacial plumes. Journal of Geophysical Research: Oceans, 120(2), 796–812.

Christoffersen, P., Mugford, R. I., Heywood, K. J., Joughin, I., Dowdeswell, J. A., Syvitski, J. P. M., Luckman, A., and Benham, T. J. (2011). Warming of waters in an east greenland fjord prior to glacier retreat: Mechanisms and connection to large-scale atmospheric conditions. The Cryosphere, 5(3), 701–714.

Cuny, J., Rhines, P. B., and Kwok, R. (2005). Davis Strait volume, freshwater and heat fluxes. Deep Sea Research Part I: Oceanographic Research Papers, 52(3), 519–542.

Curry, B., Lee, C. M., and Petrie, B. (2011). Volume, freshwater, and heat fluxes through Davis Strait, 2004–05. Journal of Physical Oceanography, 41(3), 429–436.

Curry, B., Lee, C. M., Petrie, B., Moritz, R. E., and Kwok, R. (2014). Multiyear volume, liquid freshwater, and sea ice transports through Davis Strait, 2004–10. Journal of Physical Oceanography, 44(4), 1244–1266.

de Steur, L. Pickart, R. S., Macrander, A., Våge, K., Harden, B., Jónsson, S., Østerhus, S., and Valdimarsson, H. (2017). Liquid freshwater transport estimates from the East Greenland Current based on continuous measurements north of Denmark Strait. Journal of Geophysical Research Oceans, 122(1), 93–109.

Dee, D. P., Uppala, S. M., Simmons, A. J., Berrisford, P., Poli, P., Kobayashi, S., Andrae, U., Balmaseda, M. A., Balsamo, G., Bauer, P. and Bechtold, P. (2011). The ERA-Interim reanalysis: Configuration and performance of the data assimilation system. Quarterly Journal of the Royal Meteorological Society, 137(656), 553–597.

Dowdeswell, J. A., Hogan, K. A., Cofaigh, C. Ó., Fugelli, E. M. G., Evans, J., and Noormets, R. (2014). Late Quaternary ice flow in a West Greenland fjord and cross-shelf trough system: submarine landforms from Rink Isbrae to Uummannaq shelf and slope. Quaternary Science Reviews, 92, 292–309.

Dunlap, E., and Tang, C. C. L. (2006). Modelling the mean circulation of Baffin Bay. Atmosphere-Ocean, 44(1), 99–109.

Dunlap, E., B. M., DeTracey, and Tang, C. C. L. (2007). Short-wave radiation and sea ice in Baffin Bay. Atmosphere-Ocean, 45(4), 195–210.

Edwards, A., and Edelsten, D. J. (1977). Deep Water Renewal of Loch Etive: A Three Basin Scottish Fjord. Estuarine and Coastal Marine Science, 5, 575–505.

Enderlin, E. M., Hamilton, G. S., Straneo, F., and Sutherland, D. A. (2016). Iceberg meltwater fluxes dominate the freshwater budget in Greenland's iceberg-congested glacial fjords. Geophysical Research Letters, 43, 11287–11294.

Felikson, D., Bartholomaus, T. C., Catania, G. A., Korsgaard, N. J., Kjær, K. H., Morlighem, M., Noël, B. Y. P., van den Broeke, M., Stearns, L. A., Shroyer, E. L., Sutherland, D. A., and Nash, J. D. (2017). Inland thinning on the Greenland ice sheet controlled by outlet glacier geometry. Nature Geoscience, 10, 366–369.

Fenty, I., Willis, J. K., Khazendar, A., Dinardo, S., Forsberg, R., Fukumori, I., Holland, D., Jakobsson, M., Moller, D., Morison, J. and Münchow, A. (2016) Oceans Melting Greenland: Early Results from NASA's Ocean-Ice Mission in Greenland. Oceanography, 29(4), 72–83.

Flatau, M. K., Talley, L., and Niiler, P. P. (2003). The North Atlantic Oscillation, surface current velocities, and SST changes in the subpolar North Atlantic. Journal of Climate, 16, 2355–2369.
Fratantoni, P. S., and Pickart, R. S. (2007). The western North Atlantic shelfbreak current system in summer. Journal of Physical Oceanography, 37(10), 2509–2533.

Fried, M. J., Catania, G. A., Bartholomaus, T. C., Duncan, D., Davis, M., Stearns, L. A., Nash, J. D., Shroyer, E. L., and Sutherland, D. A. (2015). Distributed subglacial discharge drives significant submarine melt at a Greenland tidewater glacier. Geophysical Research Letters, 42(21), 9328–9336.

Gladish, C. V., Holland, D. M., Rosing-Asvid, A., Behrens, J. W., and Boje, J. (2015). Oceanic boundary conditions for Jakobshavn Glacier. Part I: Variability and renewal of Ilulissat Icefjord waters, 2001–14. Journal of Physical Oceanography, 45(1), 3–32.

Gladish, C. V., Holland, D. M., and Lee, C. M. (2015). Oceanic boundary conditions for Jakobshavn Glacier. Part II: Provenance and sources of variability of Disko Bay and Ilulissat icefjord waters, 1990–2011. Journal of Physical Oceanography, 45(1), 33–63.

Grist, J. P., Josey, S. A., Boehme, L., Meredith, M. P., Laidre, K. L., Heide-Jørgensen, M. P., Kovacs, K. M., Lydersen, C., Davidson, F. J., Stenson, G. B. and Hammill, M. O. (2014). Seasonal variability of the warm Atlantic water layer in the vicinity of the Greenland shelf break. Geophysical Research Letters, 41(23), 8530–8537.

Harden, B. E., Renfrew, I. A., and Petersen, G. N. (2011). A Climatology of Wintertime Barrier Winds off Southeast Greenland. Journal of Climate, 24, 4701–4717.

Harden, B. E., and Renfrew, I. A. (2012). On the spatial distribution of high winds off southeast Greenland. Geophysical Research Letters. 39, L14806.

Harden, B. E., Straneo, F., and Sutherland, D. A. (2014). Moored observations of synoptic and seasonal variability in the East Greenland Coastal Current. Journal of Geophysical Research: Oceans, 119, 8838–8857.

Holland, D. M., and Jenkins, A. (1999). Modeling thermodynamic ice–ocean interactions at the base of an ice shelf. Journal of Physical Oceanography, 29(8), 1787–1800.

Holland, D. M., Thomas, R. H., De Young, B., Ribergaard, M. H., and Lyberth, B. (2008). Acceleration of Jakobshavn Isbrae triggered by warm subsurface ocean waters. Nature Geoscience, 1(10), 659–664.

Huppert, H. E., and Turner, J. S. (1980). Ice blocks melting into a salinity gradient. Journal of Fluid Mechanics, 100(2), 367–384.

Jackson, R. H., Straneo, F., and Sutherland, D. A. (2014). Externally forced fluctuations in ocean temperature at Greenland glaciers in non-summer months. Nature Geoscience, 7(7), 503–508.

Jackson, R. H., and Straneo, F. (2016). Heat, salt, and freshwater budgets for a glacial fjord in Greenland. Journal of Physical Oceanography, 46(9), 2735–2768.

Jackson, R. H., Shroyer, E. L., Nash, J. D., Sutherland, D. A., Carroll, D., Fried, M. J., Catania, G. A., Bartholomaus, T. C., and Stearns, L.A. (2017). Near-glacier surveying of a subglacial discharge plume: Implications for plume parameterizations. Geophysical Research Letters, 44, 6886–6894.

Jacobs, S. S., Huppert, H. E., Holdsworth, G., and D. J. Drewry. (1981). Thermohaline steps induced by melting of the Erebus Glacier tongue. Journal of Geophysical Research: Oceans and Atmospheres, 86, 6547–6555.

Jenkins, A. (2011). Convection-driven melting near the grounding lines of ice shelves and tidewater glaciers. Journal of Physical Oceanography, 41(12), 2279–2294.

Joughin, I., Alley, R. B., and Holland, D. M. (2012). Ice-sheet response to oceanic forcing. Science, 338(6111), 1172–1176.

Kawasaki, T., and Hasumi, H. (2014). Effect of freshwater from the West Greenland Current on the winter deep convection in the Labrador Sea. Ocean Modelling, 75, 51–64.

Klinck, J. M. (1996). Circulation near submarine canyons: A modeling study. Journal of Geophysical Research, 101(C1), 1211–1223.

Lilly, J. M., Rhines, P. B., Schott, F., Lavender, K., Lazier, J., Send, U., and D'Asaro, E. (2003). Observations of the Labrador Sea eddy field. Progress in Oceanography, 59(1), 75–176.

Magorrian, S. J., and Wells, A. J. (2016). Turbulent plumes from a glacier terminus melting in a stratified ocean. Journal of Geophysical Research: Oceans, 121(7), 4670–4696.

Melling, H. (2000). Exchanges of Freshwater through the Shallow Straits of the North American Arctic. In: Lewis, E. L., Jones E. P., Lemke, P., Prowse, T. D., and Wadhams, P. The Freshwater Budget of the Arctic Ocean. NATO Science Series (Series 2. Environment Security), volume 70, Springer, Dordrecht.

Moffat, C. (2014). Wind-driven modulation of warm water supply to a proglacial fjord, Jorge Montt Glacier, Patagonia. Geophysical Research Letters, 41(11), 3943–3950.

Moon, T., Joughin, I., Smith, B., Broeke, M. R., Berg, W. J., Noël, B. P. Y, and Usher, M. (2014). Distinct patterns of seasonal Greenland glacier velocity. Geophysical Research Letters, 41(20), 7209–7216.

Moon, T., Joughin, I., and Smith, B. (2015). Seasonal to multiyear variability of glacier surface velocity, terminus position, and sea ice/ice mélange in northwest Greenland. Journal of Geophysical Research: Earth Surface, 120, 818–833.

Moon, T., Sutherland, D.A., Carroll, D., Felikson, D., Kehrl, L.M., and F. Straneo. (2017). Subsurface iceberg melt key to Greenland fjord freshwater budget. Nature Geoscience, 11, 49–54.

Morlighem, M., Williams, C. N., Rignot, E., An, L., Arndt, J. E., Bamber, J. L., Catania, G. A., Chauché, N., Dowdeswell, J. A., Dorschel, B., Fenty, I., Hogan, K., Howat, I., Hubbard, A., Jakobsson, M., Jordan, T. M., Kjeldsen, K. K., Millan, R., Mayer, L., Mouginot, J., Noël, B. P. Y., Ó Cofaigh, C., Palmer, S., Rysgaard, S., Seroussi, H., Siegert, M. J., Slabon, P., Straneo, F., van den Broeke, M. R., Weinrebe, W., Wood, M., and Zinglersen, K. B. (2017). BedMachine v3: Complete bed topography and ocean bathymetry mapping of Greenland from multi-beam echo sounding combined with mass conservation. Geophysical Research Letters, 44, 11051–11061.

Mortensen, J., Lennert, K., Bendtsen, J., and Rysgaard, S. (2011). Heat sources for glacial melt in a sub-Arctic fjord (Godthåbsfjord) in contact with the Greenland Ice Sheet. Journal of Geophysical Research: Oceans, 116, C01013.

Mortensen, J., Bendtsen, J., Lennert, K., and Rysgaard, S. (2014). Seasonal variability of the circulation system in a west Greenland tidewater outlet glacier fjord, Godthåbsfjord (64 N). Journal of Geophysical Research: Earth Surface, 119(12), 2591–2603.

Myers, P. G., Donnelly, C., and Ribergaard, M. H. (2009). Structure and variability of the West Greenland Current in Summer derived from 6 repeat standard sections. Progress in Oceanography, 80(1), 93–112.

Myers, P. G., N. Kulan, and M. H. Ribergaard. (2007). Irminger Water variability in the West Greenland Current. Geophysical Research Letters, 34, L17601.

Murray, T., Scharrer, K., James, T. D., Dye, S. R., Hanna, E., Booth, A. D., Selmes, N., Luckman, A., Hughes, A. L. C., Cook, S., and Huybrechts, P. (2010). Ocean-regulation hypothesis for glacier dynamics in south-east Greenland and implications for ice-sheet mass changes. Journal of Geophysical Research, 115, F03026.

Noël, B., van de Berg, W. J., Machguth, H., Lhermitte, S., Howat, I., Fettweis, X., and van den Broeke, M. R. (2016). A daily, 1km resolution data set of downscaled Greenland ice sheet surface mass balance (1958–2015). The Cryosphere, 10(5), 2361.

Oltmanns, M., Straneo, F., Moore, G. W., and Mernild, S. H. (2014). Strong Downslope Wind Events in Ammassalik, Southeast Greenland. Journal of Climate, 27, 977–993.

Porter, D. F., Tinto, K. J., Boghosian, A., Cochran, J. R., Bell, R. E., Manizade, S. S., and Sonntag, J. G. (2014). Bathymetric control of tidewater glacier mass loss in northwest Greenland. Earth and Planetary Science Letters, 401, 40–46.

Prater, M. D. (2002). Eddies in the Labrador Sea as observed by profiling RAFOS floats and remote sensing. Journal of Physical Oceanography, 32(2), 411–427.

Ribergaard, M. H., Pedersen, S. A., Ådlandsvik, B., and Kliem, N. (2004). Modelling the ocean circulation on the West Greenland shelf with special emphasis on northern shrimp recruitment. Continental Shelf Research, 24, 1505–1519.

Rignot, E., Fenty, I., Xu, Y., Cai, C., and Kemp, C. (2015). Undercutting of marine-terminating glaciers in West Greenland. Geophysical Research Letters, 42(14), 5909–5917.

Rignot, E., Fenty, I., Xu, Y., Cai, C., Velicogna, I., Cofaigh, C. Ó., Dowdeswell, J. A., Weinrebe, W., Catania, G. and Duncan, D. (2016). Bathymetry data reveal glaciers vulnerable to ice-ocean interaction in Uummannaq and Vaigat glacial fjords, west Greenland. Geophysical Research Letters, 43(6), 2667–2674.

Rignot, E., Xu, Y., Menemenlis, D., Mouginot, J., Scheuchl, B., Li, B., Morlighem, M., Seroussi, H., van den Broeke, M., Fenty, I., Cai, C., An, L. and de Fleurian, B. (2016). Modeling of ocean-induced ice melt rates of five west Greenland glaciers over the past two decades. Geophysical Research Letters, 43, 6374–6382.

Rudels, B., Fahrbach, E., Meincke, J., Budéus, G., and Eriksson, P. (2002). The East Greenland Current and its contribution to the Denmark Strait overflow. ICES Journal of Marine Science, 59(6), 1133–1154.

Rykova, T., F. Straneo, and A. S. Bower. (2015). Seasonal and interannual variability of the West Greenland Current System in the Labrador Sea in 1993–2008. Journal of Geophysical Research: Oceans, 120, 1318–1332.

Sciascia, R., Straneo, F., Cenedese, C., and Heimbach, P. (2013). Seasonal variability of submarine melt rate and circulation in an East Greenland fjord. Journal of Geophysical Research: Oceans, 118(5), 2492–2506.

Sciascia, R., Cenedese, C., Nicoli, D., Heimbach, P., and Straneo, F. (2014). Impact of periodic intermediary flows on submarine melting of a Greenland glacier. Journal of Geophysical Research: Oceans, 119(10), 7078–7098.

She, J., and Klinck, J. M. (2000). Flow near submarine canyons driven by constant winds. Journal of Geophysical Research: Oceans, 105(C12), 28671–28694.

Slater, D. A., Nienow, P. W., Cowton, T. R., Goldberg, D. N., and Sole, A. J. (2015). Effect of near-terminus subglacial hydrology on tidewater glacier submarine melt rates. Geophysical Research Letters, 42(8), 2861–2868.

Slater, D. A., Nienow, P. W., Goldberg, D. N., Cowton, T. R., and Sole, A. J. (2017). A model for tidewater glacier undercutting by submarine melting. Geophysical Research Letters, 44(5), 2360–2368.

Skreslet, S. and Loeng, H. (1977). Deep Water Renewal and Associated Processes in Skjomen, a Fjord in North Norway. Estuarine and Coastal Marine Science, 5, 383–398.

Spall, M. A., and Pickart, R. S. (2003). Wind-driven recirculations and exchange in the Labrador and Irminger Seas. Journal of Physical Oceanography, 33(8), 1829–1845.

Spall, M. A., Jackson, R. H. and Straneo, F. (2017). Katabatic Wind-Driven Exchange in Fjords. Journal of Geophysical Research: Oceans, 122, 8246–8262.

Straneo, F., Hamilton, G. S., Sutherland, D. A., Stearns, L. A., Davidson, F., Hammill, M. O., Stenson, G. B., and Rosing-Asvid, A. (2010). Rapid circulation of warm subtropical waters in a major glacial fjord in East Greenland. Nature Geoscience, 3(3), 182–186.

Straneo, F., and Heimbach, P. (2013). North Atlantic warming and the retreat of Greenland's outlet glaciers. Nature, 504(7478), 36–43.

Straneo, F., and Cenedese, C. (2015). The dynamics of Greenland's glacial fjords and their role in climate. Annual Review of Marine Science, 7, 89–112.

Straneo, F., Hamilton, G. S., Stearns, L. A., and Sutherland, D. A. (2016). Connecting the Greenland Ice Sheet and the ocean: a case study of Helheim Glacier and Sermilik Fjord. Oceanography, 29(4), 34–45.

Sutherland, D. A., and Pickart, R. S. (2008). The East Greenland coastal current: Structure, variability, and forcing. Progress in Oceanography, 78(1), 58–77.

Sutherland, D. A., Straneo, F., Stenson, G. B., Davidson, F. J. M., Hammill, M. O., and Rosing-Asvid, A. (2013). Atlantic water variability on the SE Greenland continental shelf and its relationship to SST and bathymetry. Journal of Geophysical Research: Oceans, 118, 847–855.

Sutherland, D. A., Straneo, F., and Pickart, R. S. (2014). Characteristics and dynamics of two major Greenland glacial fjords. Journal of Geophysical Research: Oceans, 119, 3767–3791.

Svendsen, H., and R. O. Thompson. (1978), Wind-driven circulation in a fjord. Journal of Physical Oceanography, 8(4), 703–712.

Tang, C. C., Ross, C. K., Yao, T., Petrie, B., DeTracey, B. M., and Dunlap, E. (2004). The circulation, water masses and sea-ice of Baffin Bay. Progress in Oceanography, 63(4), 183–228.

Xu, Y., Rignot, E., Menemenlis, D., and Koppes, M. (2012). Numerical experiments on subaqueous melting of Greenland tidewater glaciers in response to ocean warming and enhanced subglacial discharge. Annals of Glaciology, 53(60), 229–234.

Xu, Y., Rignot, E., Fenty, I., Menemenlis, D., and Flexas, M. (2013). Subaqueous melting of Store Glacier, west Greenland from three-dimensional, high-resolution numerical modeling and ocean observations. Geophysical Research Letters, 40(17), 4648–4653.